Fixed Switching Frequency Model Predictive Control for Grid-Forming Inverters

Fernanda Carnielutti, *Member, IEEE*, Tiago Davi Curi Busarello, *Senior Member, IEEE*, Ênio Costa Resende, Qudrat Ullah, and Marcelo Godoy Simões, *Fellow, IEEE*

***Abstract*—This article proposes a Fixed Switching Frequency Model Predictive Control (FSF-MPC) for Grid-Forming Inverters (GFIs) in microgrids. The inner voltage and current loops are implemented by means of the proposed FSF-MPC, and the primary control is composed by an outer Droop and a PQ controller. Such a PQ control allows a better steady-state response and enhanced power management. The performance of the proposed FSF-MPC for grid-tied and islanded modes is demonstrated using as an example an ac microgrid equipped with 50 kVA grid-forming inverters with output *LC* filters and different loads. The microgrid is implemented in a Hardware-in-the-Loop (HIL) device, and HIL case studies are presented for grid-tied and islanded modes, with load and parametric variations and weak grid conditions. The results demonstrate the good performance of the proposed FSF-MPC approach for GFIs in microgrids, such as fast dynamic response, multivariable control, adequate load sharing between the inverters, and robustness to parametric variations and unmodeled dynamics.**

***Index Terms*—Grid-forming inverters (GFIs), microgrids, model predictive control (MPC).**

I. Introduction

THERE has been an increased demand for green energy transforming how electrical power systems must be designed and implemented in the modern distribution grids. As such, microgrids are further comprised of distributed generation units (DGs), Energy Storage Systems (ESSs), diesel gensets, consequently all the controls and communication infrastructure for power electronics, distribution lines, loads, protection system relays, communications must be now designed with a unified power systems and power electronics approach, in order to have enhanced performance.

Microgrid control is usually performed by means of a hierarchical control structure [1], [2], where the zero layer is the inner current and voltage control loops of the inverters; the primary layer performs power sharing among parallel inverters; the secondary layer is responsible for voltage and frequency regulation; and the tertiary layer performs the interaction of the microgrid with the main grid. In microgrids, some inverters must operate as grid-forming inverters (GFIs), specially in islanded mode. These GFIs synthesize the microgrid voltages and perform power sharing to feed the loads. As a result, in addition to the zero control layer, a primary controller must also be implemented for GFIs, usually by means of cascaded multiloop linear controllers such as Centralized or Distributed Control, Circular Chain Control, Average Load Sharing, Virtual Synchronous Machine (VSM), Master-Slave and Droop [3], [4], [5], [6], [7].

As discussed, linear controllers usually have cascaded multiloop structures, with an outer voltage loop and an inner current loop. In order for these loops to be decoupled, the bandwidth of the outer voltage control needs to be much smaller than that of the inner current controller; this in turn leads to bandwidth limitations that result in slow dynamic responses of the system as a whole [8]. Other limitations of these approaches include steady-state errors in the active and reactive powers, complex design procedures, the need for synchronization loops for connection and reconnection to the grid, etc. [9], [10], [11], [12], [13], [14]. The classical Droop control, e.g., can have significant steady-state errors for the active or reactive powers (respectively for resistive and inductive Droop); it also has problems to perform power sharing for nonlinear loads. Another issue is that, for controller design and implementation, the system model must be linearized around a given operational point, which can result in bad performance for different operational conditions.

On the other hand, model predictive control (MPC) is being increasingly used for microgrid control [1], [2], [3], [15]. The Finite Control Set MPC (FCS-MPC) uses the discrete-time model of the system to predict its future states [16], [17], [18]. At each sample k, a cost function is calculated for all systems inputs, and the one that minimizes the cost function is selected and implemented. The cost function can be easily

Received 11 July 2024; revised 10 January 2025; accepted 15 February 2025. Date of publication 21 February 2025; date of current version 14 April 2025. This work was supported in part by the Coordenação de Aperfeiçoamento de Pessoal de Nível Superior – Brasil (CAPES/PROEX) – Finance Code 001, and in part by INCT-GD under Grant CNPq 405054/2022-0, Grant CAPES 23038.000776/2017-54, and Grant FAPERGS 17/2551-0000517-1. Recommended for publication by Associate Editor M. Liserre. *(Corresponding author: Fernanda Carnielutti.)*

Fernanda Carnielutti is with the Federal University of Santa Maria Santa Maria and Power Electronics and Control Research Group (GEPOC), UFSM, Santa Maria 97105-900, Brazil (e-mail: fernanda.carnielutti@ufsm.br).

Tiago Davi Curi Busarello is with the Department of Control, Automation and Computing Engineering, Federal University of Santa Catarina, Blumenau 97105-900, Brazil (e-mail: tiago.busarello@ufsc.br).

Ênio Costa Resende is with the Faculty of Electrical Engineering, Federal University of Uberlândia (UFU), Uberlandia 97105-900, Brazil (e-mail: eniocostaresende@ufu.br).

Qudrat Ullah is with the School of Technology and Innovations, University of Vaasa, 65200 Vaasa, Finland (e-mail: qudrat.ullah@uwasa.fi).

Marcelo Godoy Simões is with the Department of Electrical Engineering, University of Vaasa, 65200 Vaasa, Finland (e-mail: marcelo.godoy.simoes@uwasa.fi).

Color versions of one or more figures in this article are available at https://doi.org/10.1109/TPEL.2025.3544823.

Digital Object Identifier 10.1109/TPEL.2025.3544823

designed to include multiple control objectives, in contrast to the linearization process and complex design procedures of linear controllers. Consequently, FCS-MPC can inherently consider the nonlinearities and operational constrains of the system, resulting in faster dynamic responses when compared to classical linear controllers [3].

In this context, papers were presented using FCS-MPC for GFIs, demonstrating a superior performance when compared to linear controllers. In [8], an FCS-MPC without weighting factors was proposed for GFIs with *LCL* filters, where the controlled variable is the inverter output current; however, only the zero layer was addressed, and the inverter operated with different loads only in islanded mode. In [19], an improved FCS-MPC for GFIs was presented, including an outer Droop for primary control; it was extended in [20] to include the microgrid secondary control, but only islanded mode was considered. Power sharing and transient results were presented for two inverters in parallel feeding different loads, demonstrating the faster dynamic response of FCS-MPC against linear control. In [21], an FCS-MPC for grid-tied GFIs with output virtual impedance was developed for Neutral-Point-Clamped (NPC) inverters with output *LCL* filters; however, neither power sharing nor islanded operation were addressed. In [22], a Master-Slave FCS-MPC for microgrids was proposed. The microgrid was composed by one Master NPC and two Slave NPCs. When the microgrid is connected to the main grid, the Master and the Slaves operate as grid-following inverters. When the microgrid is islanded, the Master is controlled as a GFI, while the Slaves remain grid-following inverters.

However, one of the main drawbacks of classical FCS-MPC is the variable switching frequency, that results in widespread harmonic content in the output voltages and currents. To overcome this, MPCs with fixed switching frequency (FSF-MPC) were developed. In [23], a FSF-MPC was proposed for a five-level active neutral-point clamped (5L-ANPC) converter, that also reduces the computational burden when compared to classical FCS-MPC. The Space Vector Modulated MPC (SVM^{2}PC) was presented in [24], with fast dynamic response and low computational burden. It combines control and modulation in a convex optimization problem to minimize the tracking errors of the output variables. In [24] the SVM^{2}PC was applied to GFIs, but only the inner voltage control was considered. In [25], the SVM^{2}PC of [24] was extended to include the current liming constrain in the formulation of the optimization problem, and the modified algorithm was applied to a cascaded H-Bridge inverter operating as a GFI.

An FSF-MPC for inverters in an islanded microgrid was presented in [26], addressing challenges of traditional cascaded linear controllers, such as slow transient response and susceptibility to parameter variations. In [27] and [28], a Modulated MPC (MMPC) was presented, where the duty cycles of the inverter voltage vectors were calculated using the MMPC and a carried-based PWM generated the pulses for the semiconductor switches, resulting in fixed switching frequency. A two-vector Model-Free MPC was introduced in [29] for two-level three-phase inverters, while a sequential MMPC was presented in [30], eliminating the weighting factors and achieving constant switching frequency. In [31], a Master-Slave FSF-MPC was proposed for inverters in microgrids, where the Master is a grid-following inverter when in grid-tied mode and a GFI in islanded mode, and the Slave is a grid-following inverter in both modes.

Even though various papers proposed FSF-MPCs, they have not been extensively used for GFIs and microgrids. In this context, this article proposes a FSF-MPC for GFIs in microgrids, whose initial findings were presented in [31]. The zero layer is implemented by the proposed FSF-MPC, an outer Droop is used for the voltage primary control, and an outer PQ loop allows for a better steady-state response. The proposed FSF-MPC presents fast dynamic response, multiobjective control, robustness against parametric uncertainties and variations, and adequate power sharing for grid-tied and islanded modes. As a result, it presents the main advantages of both FCS-MPC and linear controllers and modulators. The main contributions of the proposed FSF-MPC for GFIs are as follows.

1) It is a multifunctional GFI control that can, with a single cost function, control the voltages of the capacitors of the LC filters to 1) synchronize the inverter to the grid in grid-tied mode; and 2) synthesize the microgrid voltages in islanded mode; limit the current that flows through the inverter semiconductor devices; control the inverter currents to 1) perform a smooth transition from grid-tied to islanded mode and vice-versa; and 2) compensate the active and reactive power errors caused by the Droop control, allowing for a good steady-state response.
2) It brings together the advantages of FCS-MPC (fast dynamic responses) and linear controllers with PWM modulation (fixed switching frequency).
3) It does not need extra grid synchronization loops.
4) It avoids cascaded control loops, simplifying the design and implementation process and resulting in faster dynamic responses when compared to linear controllers.
5) It works in both grid-tied and islanded modes, having smooth transition from one mode to another.
6) The outer Droop control allows for GFI operation and proper power sharing for the inverters.
7) The outer PQ loop for current control can compensate the active and reactive power errors caused by the Droop control, yielding good steady-state responses for linear and nonlinear loads.
8) As the Droop control is simple, the proposed FSF-MPC can be easily extended to multiple parallel inverters.
9) It presents good performance for parametric mismatches, load variations and weak grid conditions without the need to include extra control loops. As the load and the line and grid impedances are unmodeled dynamics, the proposed FSF-MPC have robustness to unmodeled dynamics.

To validate the performance of the proposed FSF-MPC, Hardware-in-the-Loop (HIL) case studies are presented for different operational conditions of the microgrid, including grid-tied and islanded modes, dynamic load changes, weak grid and parametric variations in the *LC* filters.

The rest of this article is organized as follows. Section II describes the dynamic model of GFIs. Section III presents the

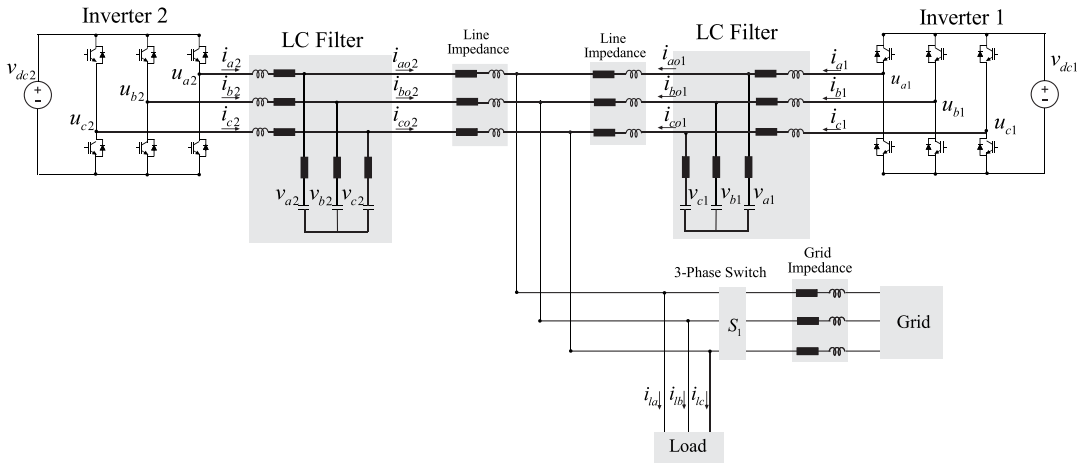

Fig. 1. Schematic of the microgrid considered as example for the proposed FSF-MPC.

classic FCS-MPC for the inner voltage control of GFIs, while Section IV presents the proposed FSF-MPC. Section V describes the proposed primary control for the microgrid. Section VI brings HIL cases studies to validate the performance of the proposed FSF-MPC. Section VII presents a comparative discussion. Finally, Section VIII concludes this article.

II. Dynamic Model of Grid-Forming Inverters

Parallel GFIs can be implemented with the proposed FSF-MPC strategy that will be described in Section IV, considering initially a three-phase microgrid composed of two inverters with *LC* filters, a load, line impedances, a switch, and the main grid, as presented in Fig. 1. Such a microgrid could be grid connected or intentionally islanded with switch S1; a communication link between the microgrid central controller and the inverters is also needed, but it is out of the scope of this work and will be reported in another paper.

First, let us present the discrete-time dynamic model of the GFIs. The equations below are valid for both inverters, and describe the inverter-side currents and capacitor voltages in $\alpha\beta$ coordinates. The amplitude invariant Clarke transformation was used to obtain the model in $\alpha\beta$ coordinates

$$\begin{bmatrix} i_\alpha(k+1) \\ i_\beta(k+1) \end{bmatrix} = (1 - \frac{RT_s}{L}) \begin{bmatrix} 1 & 0 \\ 0 & 1 \end{bmatrix} \begin{bmatrix} i_\alpha(k) \\ i_\beta(k) \end{bmatrix} + \frac{T_s}{L} \begin{bmatrix} 1 & 0 \\ 0 & 1 \end{bmatrix} \begin{bmatrix} u_\alpha(k) \\ u_\beta(k) \end{bmatrix} - \frac{T_s}{L} \begin{bmatrix} 1 & 0 \\ 0 & 1 \end{bmatrix} \begin{bmatrix} v_\alpha(k) \\ v_\beta(k) \end{bmatrix} \quad (1)$$

$$\begin{bmatrix} v_\alpha(k+2) \\ v_\beta(k+2) \end{bmatrix} = \begin{bmatrix} v_\alpha(k+1) \\ v_\beta(k+1) \end{bmatrix} + \frac{T_s}{C} \begin{bmatrix} 1 & 0 \\ 0 & 1 \end{bmatrix} \begin{bmatrix} i_\alpha(k+1) \\ i_\beta(k+1) \end{bmatrix} - \frac{T_s}{C} \begin{bmatrix} 1 & 0 \\ 0 & 1 \end{bmatrix} \begin{bmatrix} i_{o\alpha}(k+1) \\ i_{o\beta}(k+1) \end{bmatrix} \quad (2)$$

or

$$\mathbf{i}_{\alpha\beta}(k+1) = \mathbf{A}_i \mathbf{i}_{\alpha\beta}(k) + \mathbf{B}_i \mathbf{u}_{\alpha\beta}(k) - \mathbf{F}_i \mathbf{v}_{\alpha\beta}(k) \quad (3)$$

$$\mathbf{v}_{\alpha\beta}(k+2) = \mathbf{v}_{\alpha\beta}(k+1) + \mathbf{B}_c \mathbf{i}_{\alpha\beta}(k+1) - \mathbf{F}_c \mathbf{i}_{o\alpha\beta}(k+1) \quad (4)$$

where $\mathbf{i}_{\alpha\beta}$ and $\mathbf{i}_{o\alpha\beta}$ are the inverter-side and output currents, $\mathbf{u}_{\alpha\beta}$ are the inverter output voltages, $\mathbf{v}_{\alpha\beta}$ are the filter capacitor voltages, T_s is the sampling period and L, C and R are the filter parameters. The output currents $\mathbf{i}_{o\alpha\beta}$ are measured after the filter and considered as disturbances. Eqs. (1)–(2) were obtained by discretizing the continuous-time model by the Forward Euler discretization method. As the MPC usually is implemented in a Digital Signal Processor (DSP) the implementation delay must be considered as

$$\mathbf{i}_{\alpha\beta}(k+2) = \mathbf{A}_i \mathbf{i}_{\alpha\beta}(k+1) + \mathbf{B}_i \mathbf{u}_{\alpha\beta}(k+1) - \mathbf{F}_i \mathbf{v}_{\alpha\beta}(k+1) \quad (5)$$

$$\mathbf{v}_{\alpha\beta}(k+3) = \mathbf{v}_{\alpha\beta}(k+2) + \mathbf{B}_c \mathbf{i}_{\alpha\beta}(k+2) - \mathbf{F}_c \mathbf{i}_{o\alpha\beta}(k+2). \quad (6)$$

III. Classical FCS-MPC for GFIs

Some of the main control objectives of GFIs are: 1) to limit the inverter-side currents; and 2) to control the filter capacitor voltages. Considering this multiobjective control problem, a cost function for classical FCS-MPC for GFIs can be

$$g_j = (\mathbf{v}^*_{\alpha\beta}(k+3) - \mathbf{v}_{j\alpha\beta}(k+3))^2 + I_{lim} \quad (7)$$

where $\mathbf{v}^*_{\alpha\beta}$ are the filter voltage references (the generation of the voltage references will be described in Section V) and $j = 0, \ldots 7$ are the eight voltage vectors of a three-phase two-level inverter. The term I_{lim} is included to limit the amplitude of the inverter-side currents and avoid damage to the semiconductor devices. If the norm of the calculated $\mathbf{i}_{j\alpha\beta}$ for a given inverter voltage vector is greater than the inverter maximum current, I_{lim} assumes a large value, and zero otherwise [19], [20].

In a classical FCS-MPC, at each sampling instant k, the inverter-side currents and the filter capacitor voltages are predicted for all inverter voltage vectors using (5)–(6), and cost function (7) is evaluated. Then, the inverter voltage vector that results in the minimum value of (7) is chosen and implemented

TABLE I
SWITCHING SEQUENCES FOR EACH SECTOR OF THE SV DIAGRAM

Sector	Switching Sequence
S1	$\mathbf{v^0 v^1 v^2 v^7}$
S2	$\mathbf{v^0 v^3 v^2 v^7}$
S3	$\mathbf{v^0 v^3 v^4 v^7}$
S4	$\mathbf{v^0 v^5 v^4 v^7}$
S5	$\mathbf{v^0 v^5 v^6 v^7}$
S6	$\mathbf{v^0 v^1 v^6 v^7}$

TABLE II
NORMALIZED INVERTER VOLTAGE VECTORS

Vector	Switching States
$\mathbf{v^0}$	$[0 \quad 0 \quad 0]^T$
$\mathbf{v^1}$	$[1 \quad 0 \quad 0]^T$
$\mathbf{v^2}$	$[1 \quad 1 \quad 0]^T$
$\mathbf{v^3}$	$[0 \quad 1 \quad 0]^T$
$\mathbf{v^4}$	$[0 \quad 1 \quad 1]^T$
$\mathbf{v^5}$	$[0 \quad 0 \quad 1]^T$
$\mathbf{v^6}$	$[1 \quad 0 \quad 1]^T$
$\mathbf{v^7}$	$[1 \quad 1 \quad 1]^T$

in the next sampling period T_s. Even though the FCS-MPC is a simple and effective control strategy, it results in variable switching frequency. Therefore, to solve this issue, the proposed FSF-MPC is described in the next Section.

IV. PROPOSED FSF-MPC FOR GFIS

To achieve fixed switching frequency, the inverter voltage vectors must be modulated in a way similar to a carrier-based Pulse-Width Modulation (PWM) or Space Vector Modulation (SVM). In the proposed FSF-MPC, a switching sequence is defined offline for each of the six sectors of the Space Vector diagram of the inverters of Fig. 1. The switching sequences are comprised of two nonnull voltage vectors and both redundancies of the null vector, and are designed for $T_s/2$, i.e., half the carrier period (a triangular carrier is considered, with sampling at the underflow and period match). The switching sequences and the normalized inverter voltage vectors are respectively presented in Tables I and II.

For the proposed FSF-MPC, for each T_s, first the inverter-side currents and the filter capacitor voltages are predicted for all inverter voltage vectors through (5)–(6), and cost function (7) is evaluated. The next step is the selection of the sector and its corresponding switching sequence to be implemented by the inverter. The duty cycles for the three vectors in each sector are calculated as described in [23]

$$d_1 = \frac{g_2 g_3}{G} \quad d_2 = \frac{g_1 g_3}{G} \quad d_3 = \frac{g_1 g_2}{G} \tag{8}$$

$$G = (g_2 g_3 + g_1 g_3 + g_2 g_1) \tag{9}$$

where g_1, g_2, and g_3 are the costs of the vectors of a given sector, and $d_1 + d_2 + d_3 = 1$. The sector cost function is

$$g_s = d_1 g_1 + d_2 g_2 + d_3 g_3 \tag{10}$$

where $s = 1 \ldots 6$ are the six sectors of the SV diagram. The sector with the lowest value of g_s is selected and its respective switching sequence is implemented over T_s, resulting in fixed switching frequency. This procedure is depicted in the block diagram presented in Fig. 2.

V. MICROGRID PRIMARY CONTROL

As mentioned in the Introduction, the control of a microgrid can be implemented by a hierarchical strategy. However, it is well known that standard grid-forming strategies based on linear controllers can have limitations [9], [10], [11], [12], [13], [14], such as slow dynamic responses. In order to overcome these problems, in this article an outer Droop and a PQ controller are used for the primary control of the microgrid, and the inner FSF-MPC described in Section IV provides a faster dynamic response to the system [19], [20]. The Droop law can be written as

$$v(k) = v_{nom} - k_p(P^* - P(k)) \tag{11}$$

$$\omega(k) = \omega_{nom} + k_q(Q^* - Q(k)) \tag{12}$$

where v is the amplitude of the voltage reference, v_{nom} is the nominal amplitude voltage, ω is the frequency reference, ω_{nom} is the nominal frequency, k_p and k_q are the Droop coefficients, P^* and Q^* are the active and reactive power references, and P and Q are the inverter instantaneous active and reactive powers calculated as

$$P(k) = \frac{3}{2}(v_\alpha(k) i_{o\alpha}(k) + v_\beta(k) i_{o\beta}) \tag{13}$$

$$Q(k) = \frac{3}{2}(v_\beta(k) i_{o\alpha}(k) - v_\alpha(k) i_{o\beta}(k)). \tag{14}$$

No filters are needed for P and Q when the inner control is implemented with MPC [19], [20]. Then, the voltage references can be defined as

$$v^*_\alpha(k) = v(k)\cos(\omega^* T_s) - R_v i_{o\alpha}(k) \tag{15}$$

$$v^*_\beta(k) = v(k)\sin(\omega^* T_s) - R_v i_{o\beta}(k) \tag{16}$$

where R_v is a virtual impedance. A virtual resistor is implemented, as it does not vary with the frequency as a virtual inductor. It also provides damping to the microgrid, contributing to system stability [19], [32]. As seen in (6), the voltage references must be calculated for $k+3$. Therefore, (15)–(16) are extrapolated to $k+3$ as

$$v^*_\alpha(k+3) = v_\alpha(k)\cos(3\omega T_s) - v_\beta(k)\sin(3\omega T_s) \tag{17}$$

$$v^*_\beta(k+3) = v_\beta(k)\cos(3\omega T_s) + v_\alpha(k)\sin(3\omega T_s). \tag{18}$$

A classical GFI controller usually generates only the voltage references for the inverter. However, these implementations can have other problems besides slow dynamic responses, such as steady-state errors for the active and/or reactive powers, problems to perform power sharing for nonlinear loads, grid synchronization, etc. [9], [10], [11], [12], [13], [14]. Therefore, recent papers have explored the integration of voltage and current control to achieve better performance for GFIs [33], [34], [35], [36], [37], [38], usually by integrating GFI and grid-following functionalities in the same controller. In the proposed

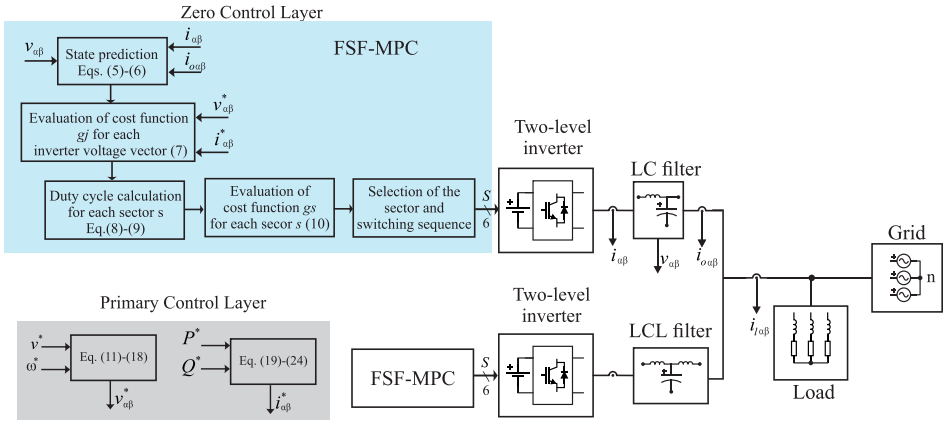

Fig. 2. Block diagram of the proposed FSF-MPC for parallel grid-forming inverters.

FSF-MPC, this can be achieved by including a term in cost function (7) that is responsible for controlling the inverter-side currents as

$$g_j = \lambda_1(\mathbf{v}^*_{\alpha\beta}(k+3) - \mathbf{v}_{j\alpha\beta}(k+3))^2 + \lambda_2(\mathbf{i}^*_{\alpha\beta}(k+2) - \mathbf{i}_{j\alpha\beta}(k+2))^2 + I_{lim} \quad (19)$$

where λ_1 and λ_2 are weighting factors and $\mathbf{i}^*_{\alpha\beta}$ are the inverter-side current references. The control of the inverter-side currents allows the control of the active and reactive powers injected into the grid or load, improving the steady-state performance of the Droop controller with the proposed FSF-MPC, as will be demonstrated in Section VII. To generate the current references, an open-loop PQ control is used [39]

$$i^*_{o\alpha}(k) = \frac{2}{3}\frac{1}{v^2_\alpha(k) + v^2_\beta(k)}(v_\alpha(k)P^* + v_\beta(k)Q^*) \quad (20)$$

$$i^*_{o\beta}(k) = \frac{2}{3}\frac{1}{v^2_\alpha(k) + v^2_\beta(k)}(v_\beta(k)P^* - v_\alpha Q^*(k)). \quad (21)$$

For proper power sharing, P^* and Q^* for each inverter are set in this article as half the total active and reactive powers demanded from the load. These power references can come from the secondary control layer of the microgrid, that is out of the scope of this article. To obtain the inverter-side currents, the reactive power of the *LC* filter must be compensated

$$i^*_\alpha(k) = i^*_{o\alpha}(k) - \omega C v_\beta(k) \quad (22)$$

$$i^*_\beta(k) = i^*_{o\beta}(k) + \omega C v_\alpha(k). \quad (23)$$

Then, the references are extrapolated to $(k+2)$

$$i^*_\alpha(k+2) = i^*_\alpha(k)\cos(2\omega T_s) - i^*_\beta(k)\sin(2\omega T_s) \quad (24)$$

$$i^*_\beta(k+2) = i^*_\beta(k)\cos(2\omega T_s) + i^*_\alpha(k)\sin(2\omega T_s). \quad (25)$$

Therefore, the proposed FSF-MPC is a multifunctional GFI control that can, with a single cost function, control the voltages of the capacitors of the *LC* filters to: 1) synchronize the inverter to the grid in grid-tied mode; and 2) synthesize the microgrid voltages in islanded mode; limit the current that flows through the inverter semiconductor devices; control the inverter currents to 1) perform a smooth transition from grid-tied to islanded mode and vice-versa; and 2) compensate the active and reactive power errors caused by the Droop control, allowing for a good steady-state response for both parallel inverters, as will be demonstrated in the next section.

TABLE III
SYSTEM PARAMETERS FOR THE CASE STUDIES

Parameter	Value
Total dc-link voltage	800 V
Rated power	50 kVA
LC filter	500 μH; 300 μF
Filter parasitic resistance R_f	0.012 Ω
Filter damping resistor	0.2 Ω
Line impedance	Z_l = 20 μH, 0.01 Ω
Grid impedance (strong grid)	Z_g = 1 mH, 0.3 Ω
Grid X/R (strong grid)	1.05
Grid impedance (weak grid)	Z_g = 10 mH, 0.01 Ω
Grid X/R (weak grid)	314.15
Grid voltage	220 Vrms; 50 Hz
Sampling frequency f_s	20 kHz
Switching frequency f_s	10 kHz
R_v	0.006 Ω

VI. CASE STUDIES

To validate the proposed FSF-MPC, the microgrid of Fig. 1 was implemented in a Typhoon HIL 604 HIL device. The system parameters are shown in Table III, and apply to both GFIs. The controllers were implemented in the ARM core of Typhoon HIL 604, including the implementation delay. The weighting factors are $\lambda_1 = 10000$ and $\lambda_2 = 4000$ for grid-tied mode and $\lambda_1 = 2000$ and $\lambda_2 = 400$ for islanded mode. A strong grid was considered, with $R = 0.3\Omega$ and $L = 1$ mH and X/R ratio of 1.05. Case studies for different operational conditions are provided to demonstrate the good performance of the proposed FSF-MPC.

A. Transition From Grid-Tied to Islanded Mode, Load Changes, and Transition From Islanded to Grid-Tied Mode

In the first case study, the microgrid transitions from grid-tied to islanded mode and vice-versa, and load changes are applied

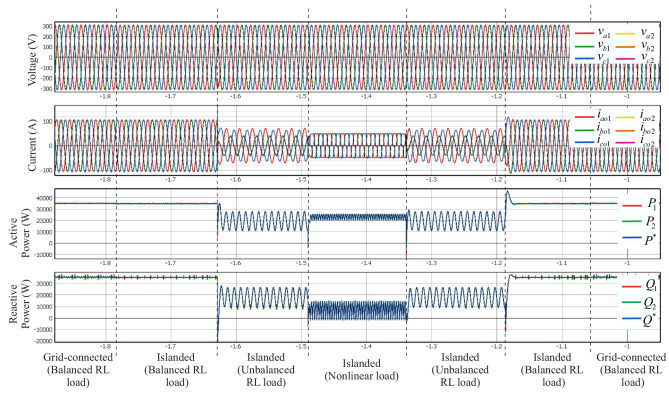

Fig. 3. Filter capacitor voltages, grid-side currents, active and reactive powers of both inverters for the proposed FSF-MPC.

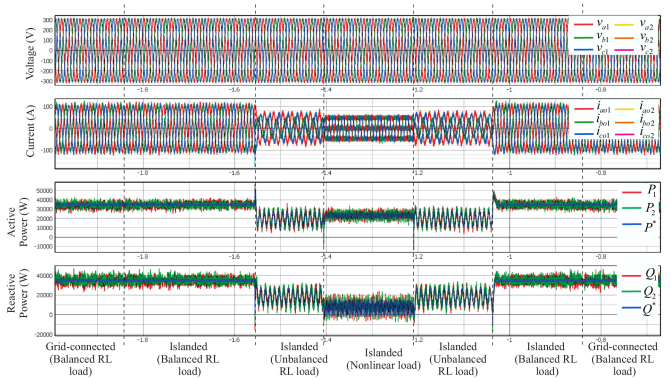

Fig. 4. Filter capacitor voltages, grid-side currents, active and reactive powers of both inverters for a classical FCS-MPC.

in islanded mode. The results are depicted in Fig. 3, that shows, from top to bottom, the filter capacitor voltages, grid-side currents, active and reactive powers of both GFIs, and active and reactive power references (the voltages and currents of both GFIs are superimposed). First, the microgrid is connected to the grid and to a balanced three-phase RL load ($R = 1.03\Omega$ and $L = 3.3$ mH). Then, the microgrid is islanded, and the following load changes are performed:

1) unbalanced RL load ($R_a = 1.03\Omega$ and $L_a = 3.3$ mH, $R_b = 4\Omega$ and $L_b = 10$ mH and $R_c = 2\Omega$ and $L_c = 6$ mH);
2) nonlinear load (three-phase diode rectifier with inductive input filter of 1 mH and an RL load equal to $R = 5\Omega$ and $L = 5$ mH;
3) same unbalanced RL load;
4) same balanced RL load. Finally, the microgrid is again connected to the main grid.

The results presented in Fig. 3 demonstrate that the GFIs properly perform power sharing, providing the total load power. The fast transient response of both inverters is observed in all waveforms, as their active and reactive powers speedily converge to the new set points after the load changes; consequently, the currents and voltages also present fast dynamic responses. As seen in (5) and (6), the load is not included in the model; thus, these results demonstrate the good performance of the proposed FSF-MPC for unmodeled dynamics.

1) Comparison of the Proposed FSF-MPC and Classical FCS-MPC: To demonstrate the superior performance of the proposed FSF-MPC over classical FCS-MPC, a comparative analysis is presented here. The classical FCS-MPC was implemented with the same parameters of Table III and the same weighting factors. As it has variable switching frequency, the value of f_s shown in Table III does not apply. The results are shown in Fig. 4, presenting the same waveforms and events as Fig. 3. Even though the fast transient response is maintained, the ripple on the active and reactive powers, as well as on the currents, is much higher than for the proposed FSF-MPC; this results in a degraded steady-state performance, leading to higher Total Harmonic Distortion (THD).

The THD of the grid-side currents for the proposed FSF-MPC and the classical FCS-MPC for grid-tied mode are shown in Table IV, with the balanced RL load as example. The fixed switching frequency is demonstrated by the spectra of the inverter output line-to-line voltages, measured before the *LC* filters. Fig. 5 shows the FFTs of the output line-to-line voltages v_{ab} and v_{bc} for the proposed FSF-MPC. The first significant set of harmonics is at 10 kHz, validating the fixed switching frequency. On the other hand, Fig. 6 shows the FFTs of v_{ab} and v_{bc} for the

TABLE IV
THD OF THE GRID-SIDE CURRENTS FOR THE CLASSICAL FCS-MPC FOR GRID-TIED MODE WITH BALANCED RL LOAD

Grid-side currents	FCS-MPC	Proposed FSF-MPC
i_{a1}	9.05%	0.94%
i_{b1}	9.06%	0.93%
i_{c1}	8.48%	0.78%
i_{a2}	8.31%	0.79%
i_{b2}	8.46%	0.97%
i_{c2}	8.43%	0.99%

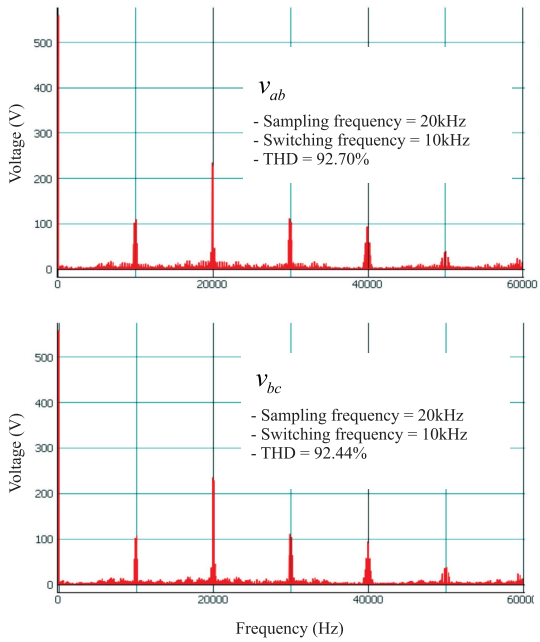

Fig. 5. FFT of voltages v_{ab} and v_{bc} for the proposed FSF-MPC.

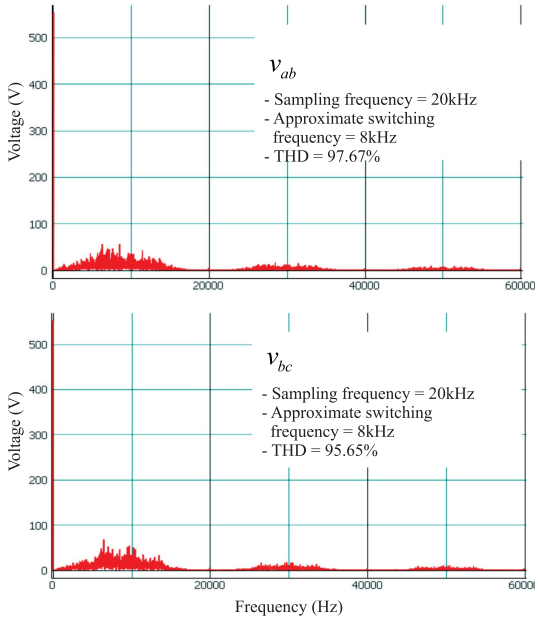

Fig. 6. FFT of voltages v_{ab} and v_{bc} for a classical FCS-MPC.

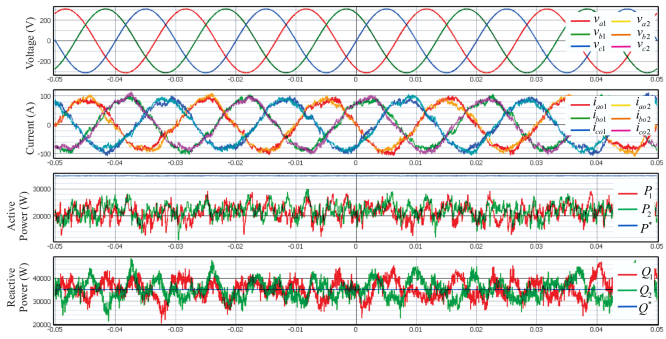

Fig. 7. Filter capacitor voltages, grid-side currents, active and reactive powers of both inverters for the proposed FSF-MPC without the outer PQ loop.

classical FCS-MPC, where the widespread harmonic content is evident. Even though the THDs of the output line-to-line voltages are similar for both MPCs, the fixed f_s of the proposed FSF-MPC allows for better filtering of the harmonics. The current THD of the proposed FSF-MPC is considerably smaller than for the classical FCS-MPC.

2) Comparison of the Proposed FSF-MPC With and Without PQ Control: Now, let us demonstrate that the inclusion of the outer PQ control in the primary layer improves the steady-state response of the FSF-MPC. To do so, the proposed FSF-MPC was implemented only with the Droop control, using cost function (7). As an example, Fig. 7 shows the results of this implementation for grid-tied mode and balanced RL load. It can be seen that, for the system considered, the inverter output currents are distorted, and there is a high steady-state error for the active power (which is expected for resistive Droop). On the other hand, Fig. 8 shows the same results for the proposed FSF-MPC with the outer PQ loop, using cost function (19). In this case, the current control term in (19) compensates the previous problems, achieving low

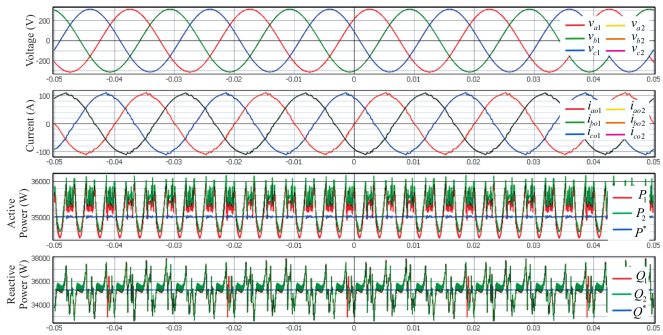

Fig. 8. Filter capacitor voltages, grid-side currents, active and reactive powers of both inverters for the proposed FSF-MPC with the outer PQ loop.

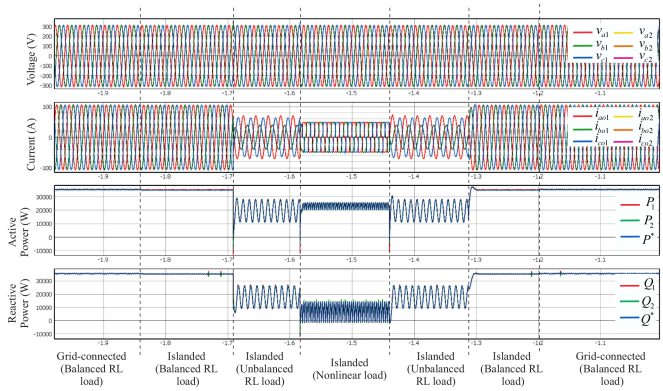

Fig. 9. Filter capacitor voltages, grid-side currents, active and reactive powers of both inverters for the proposed FSF-MPC for weak grid.

steady-state error for the active power. The same holds for the reactive power, where it is seen that the ripple is smaller than for the FSF-MPC only with Droop. The calculated steady state error for the active powers of the FSF-MPC only with Droop is 37.27% and 39.48% for inverters 1 and 2, respectively, and, for the reactive powers, 0.74% for both inverters. In comparison, the steady state error for the active powers of the FSF-MPC with Droop and PQ control are 0.86% and 0.43% for inverters 1 and 2, respectively, and, for the reactive powers, 0.40% and 0.11% for inverters 1 and 2. Therefore, we can see that the proposed FSF-MPC with Droop and PQ control performs better than the same FSF-MPC implemented only with Droop.

B. Operation With Weak Grid

To verify the performance of the proposed FSF-MPC for weak grid conditions, a weak grid with impedance $R = 0.01\,\Omega$ and $L = 10$ mH is considered, with X/R ratio of 314.15. The results are shown in Fig. 9, that present the same transient events and waveforms as Fig. 3. It can be seen that the proposed FSF-MPC is stable and presents good dynamic and steady-state performances for weak grids. The grid impedance is also an unmodeled dynamics, as it is not included in (5) and (6). These results demonstrate the good performance of the proposed FSF-MPC with respect to grid unmodeled dynamics.

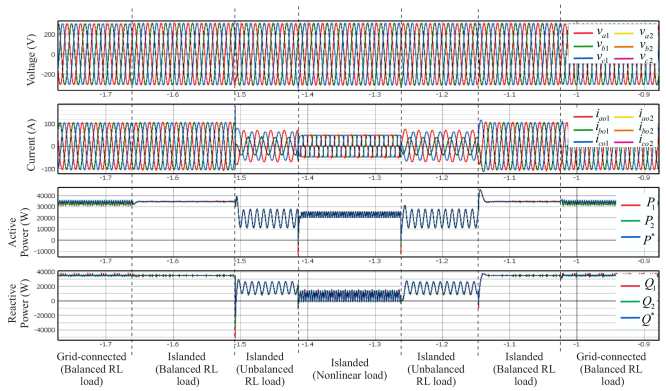

Fig. 10. Filter capacitor voltages, grid-side currents, active and reactive powers of both inverters for the proposed FSF-MPC for increased filter parameters.

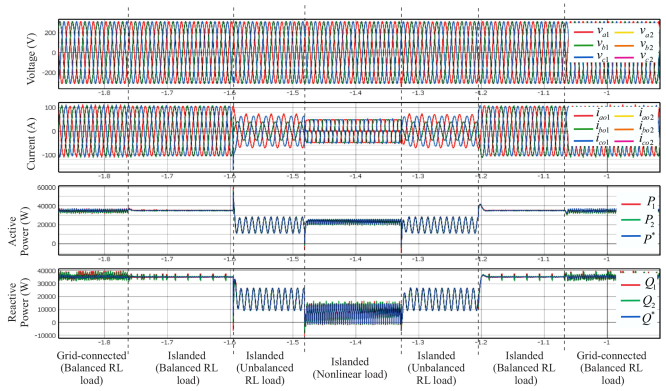

Fig. 11. Filter capacitor voltages, grid-side currents, active and reactive powers of both inverters for the proposed FSF-MPC for decreased filter parameters.

C. Parametric Variations in the LC Filter

To verify the robustness of the proposed FSF-MPC to parametric variations, two examples are shown, in which the filter parameters are increased and decreased in the system, but are kept equal to the nominal values in (5)–(6). These results are presented in Figs. 10 and 11, that show the same waveforms and events as Fig. 3. First, Fig. 10 shows the results for an increase in the filter parameters; the nominal values are presented in Table III, and the increased ones are $R = 0.018\,\Omega$, $L = 550\,\mu$H, and $C = 350\,\mu$F. In this case, higher ripples appear at the currents and voltages, that are reflected in the active and reactive powers. However, the transient response is still satisfactory. Fig. 11 presents the same results, but now with the filter parameters decreased to $R = 0.01\,\Omega$, $L = 450\,\mu$H, and $C = 250\,\mu$F. Again, the inverters operate properly for all conditions. The main differences now are seen in the higher ripple on the active and reactive powers, as the filter inductance is smaller than the nominal value. Higher distortions also appear at the currents and voltages. However, the system in stable for both cases, and these results demonstrate that the proposed FSF-MPC is robust to parametric variations.

VII. Comparative Analysis

In this section, the proposed FSF-MPC will be qualitatively compared to the hybrid GFI controllers cited in Section IV. First, in [33], a multifunctional GFI control with a disturbance observer was proposed with three different modes: 1) grid-forming; 2) grid-following; and 3) current control. It does not require extra synchronization loops, as this is incorporated in the disturbance observer. The proposed FSF-MPC also does not require an extra synchronization loop, as this is achieved by the Droop and the PQ control. In [33], the three control modes were incorporated in the same disturbance observer, which is analogous to cost function (19) with multiple control objectives of the proposed FSF-MPC. However, as [33] is based on classical linear controllers, the active and reactive power dynamic responses are slower when compared to MPC. Also, in [33] the islanded operation of the GFIs is not discussed, nor the operation of multiple inverters in parallel.

In [34], a method to control parallel inverters that operate in grid-following and grid-forming modes was proposed. The controller uses two synchronized semiparallel control paths, and when the grid-following inverters are disconnected from the grid, they transition to GFI mode. In [34], the multiple control modes were not integrated in a single control as in [33] and in the proposed FSF-MPC. Other disadvantages of [34] are that it requires a synchronization loop, which is avoided by the proposed FSF-MPC, and the linear controllers have slower dynamic responses when compared to MPC.

In [35], multiple linear controllers were cascaded to perform direct and indirect control for an inverter that can operate as grid-forming and grid-following. The indirect grid-following control allows the inverter to act like a current source; for grid-forming, it limits the currents through the semiconductor devices. In contrast, the direct control eliminates the inner current loop. The power is directly managed in grid-following mode, while voltage and frequency are regulated in grid-forming mode through the outer loops. Comparing [35] to the proposed FSF-MPC, the multiple cascaded linear controllers result in slower dynamic responses for the system. In addition, [35] needs an extra synchronization loop.

In [36], a modified GFI based on VSM was proposed. An extra synchronization loop is added to the VSM to achieve smooth transition to grid-tied mode. In comparison, the proposed FSF-MPC does not need extra synchronization loops, and the current control makes sure that no high inrush currents will arise. In addition, in [36] the analysis of multiple inverters in parallel was not presented.

In [37], a GFI control for parallel inverters was proposed to control active and reactive powers, perform smooth transition from grid–tied to islanded mode and vice-versa, and perform autonomous power sharing. A cascaded control structure is used, and the reconnection to the grid is done by a central controller with a synchro-check relay at the point-of-common-coupling of the microgrid. In contrast, the proposed FSF-MPC achieves faster dynamic responses, as cascaded control loops are avoided by the use of a single cost function, simplifying the design and implementation process of the controller.

Finally, in [38], a hybrid control strategy was proposed that incorporates both PLL and Droop. It regulates the active power by adjusting the phase angle across the filter inductance, similar to a VSM. As it is a hybrid controller, it presents both grid-forming and grid-following characteristics, similar to what is

accomplished by cost function (20) of the proposed FSF-MPC. However, [38] is also implemented with cascaded linear voltage and current controllers, resulting in slower dynamic responses when compared to MPC.

VIII. Conclusion

This article proposed a FSF-MPC for GFIs in microgrids. The zero control layer is implemented by means of the proposed FSF-MPC, and the primary control is composed by an outer Droop and a PQ controller. The inclusion of the PQ control allows for a better steady-state response of the system. To validate the proposed FSF-MPC, Hardware-in-the-Loop case studies were presented for grid-tied and islanded modes, with load and parametric variations and weak grid conditions. The results demonstrated the excellent performance of the proposed FSF-MPC approach for GFIs in microgrids, such as fast dynamic response, multivariable control, adequate load sharing among the inverters and robustness to parametric uncertainties and unmodeled dynamics.

References

[1] J. Hu, Y. Shan, J. M. Guerrero, A. Ioinovici, K. W. Chan, and J. Rodriguez, "Model predictive control of microgrids–an overview," *Renewable Sustain. Energy Rev.*, vol. 136, 2021, Art. no. 110422.

[2] Z. Zhang et al., "Advances and opportunities in the model predictive control of microgrids: Part I–Primary layer," *Int. J. Elect. Power Energy Syst.*, vol. 134, 2022, Art. no. 107411.

[3] J. G. J. Hu and S. Islam, *Model Predictive Control for Microgrids - From Power Electronics Converters to Energy Management*. IET - Inst. Eng. Technol., 2021. [Online]. Available: https://digital-library.theiet.org/doi/book/10.1049/pbpo199e

[4] J. Hu, Y. Shan, K. W. Cheng, and S. Islam, "Overview of power converter control in micro grids challenges, advances, and future trends," *IEEE Trans. Power Electron.*, vol. 37, no. 8, pp. 9907–9922, Aug. 2022.

[5] O. Babayomi, Y. Li, Z. Zhang, R. Kennel, and J. Kang, "Overview of model predictive control of converters for islanded AC microgrids," in *Proc. IEEE 9th Int. Power Electron. Motion Control Conf.*, Nov. 2020, pp. 1023–1028.

[6] B. Fan et al., "A novel droop control strategy of reactive power sharing based on adaptive virtual impedance in microgrids," *IEEE Trans. Ind. Electron.*, vol. 69, no. 11, pp. 11335–11347, Nov. 2022.

[7] Y. Han, H. Li, P. Shen, E. A. A. Coelho, and J. M. Guerrero, "Review of active and reactive power sharing strategies in hierarchical controlled microgrids," *IEEE Trans. Power Electron.*, vol. 32, no. 3, pp. 2427–2451, Mar. 2017.

[8] H. A. Young, V. A. Marin, C. Pesce, and J. Rodriguez, "Simple finite-control-set model predictive control of grid-forming inverters with LCL filters," *IEEE Access*, vol. 8, pp. 81246–81256, 2020.

[9] W. Zhang, W. Wang, H. Liu, and D. Xu, "A disturbance rejection control strategy for droop-controlled inverter based on super-twisting algorithm," *IEEE Access*, vol. 7, pp. 27037–27046, 2019.

[10] Y. Jiang, R. Pates, and E. Mallada, "Dynamic droop control in low-inertia power systems," *IEEE Trans. Autom. Control*, vol. 66, no. 8, pp. 3518–3533, Aug. 2021.

[11] D. Pan, X. Wang, F. Liu, and R. Shi, "Transient stability of voltage-source converters with grid-forming control: A design-oriented study," *IEEE Trans. Emerg. Sel. Topics Power Electron.*, vol. 8, no. 2, pp. 1019–1033, Jun. 2020.

[12] Y. Deng, Y. Tao, G. Chen, G. Li, and X. He, "Enhanced power flow control for grid-connected droop-controlled inverters with improved stability," *IEEE Trans. Ind. Electron.*, vol. 64, no. 7, pp. 5919–5929, Jul. 2017.

[13] N. Mohammed, H. Udawatte, W. Zhou, D. J. Hill, and B. Bahrani, "Grid-forming inverters: A comparative study of different control strategies in frequency and time domains," *IEEE Open J. Ind. Electron. Soc.*, vol. 5, pp. 185–214, 2024.

[14] A. Narula, M. Bongiorno, M. Beza, J. R. Svensson, X. Guillaud, and L. Harnefors, "Impact of steady-state grid-frequency deviations on the performance of grid-forming converter control strategies," in *Proc. 22nd Eur. Conf. Power Electron. Appl.*, 2020, pp. P.1–P.10.

[15] O. Babayomi et al., "Advances and opportunities in the model predictive control of microgrids: Part II–Secondary and tertiary layers," *Int. J. Elect. Power Energy Syst.*, vol. 134, 2022, Art. no. 107339.

[16] J. Rodriguez et al., "State of the art of finite control set model predictive control in power electronics," *IEEE Trans. Ind. Informat.*, vol. 9, no. 2, pp. 1003–1016, May 2013.

[17] S. Vazquez, J. Rodriguez, M. Rivera, L. G. Franquelo, and M. Norambuena, "Model predictive control for power converters and drives: Advances and trends," *IEEE Trans. Ind. Electron.*, vol. 64, no. 2, pp. 935–947, Feb. 2017.

[18] P. Karamanakos, E. Liegmann, T. Geyer, and R. Kennel, "Model predictive control of power electronic systems: Methods, results, and challenges," *IEEE Open J. Ind. Appl.*, vol. 1, pp. 95–114, 2020.

[19] T. Dragičević, "Model predictive control of power converters for robust and fast operation of ac microgrids," *IEEE Trans. Power Electron.*, vol. 33, no. 7, pp. 6304–6317, Jul. 2018.

[20] C. Zheng, T. Dragičević, and F. Blaabjerg, "Model predictive control-based virtual inertia emulator for an islanded alternating current microgrid," *IEEE Trans. Ind. Electron.*, vol. 68, no. 8, pp. 7167–7177, Aug. 2021.

[21] J. Chhor and B. Lammersmann, "Predictive voltage control for grid-forming power converters with virtual output impedance," in *Proc. 47th Annu. Conf. IEEE Ind. Electron. Soc.*, 2021, pp. 1–7.

[22] F. Carnielutti, M. Aly, M. Norambuena, J. Hu, J. Guerrero, and J. Rodriguez, "A master-slave model predictive control approach for microgrids," *IEEE Trans. Power Electron.*, vol. 40, no. 1, pp. 540–550, Jan. 2025.

[23] Y. Yang et al., "Computationally efficient model predictive control with fixed switching frequency of five-level ANPC converters," *IEEE Trans. Ind. Electron.*, vol. 69, no. 12, pp. 11903–11914, Dec. 2022.

[24] D. Schuetz et al., "Space vector modulated model predictive control for grid-tied converters," *IEEE Trans. Ind. Informat.*, vol. 19, no. 1, pp. 414–425, Jan. 2023.

[25] J.-M. De Paris, V. F. Montagner, D. Martins Lima, F. de Morais Carnielutti, and H. Pinheiro, "Geometrical modulated model predictive control with current limiting for power converters," *IEEE Trans. Emerg. Sel. Topics Power Electron.*, vol. 11, no. 5, pp. 4749–4760, Oct. 2023.

[26] A. Villalón, C. Muñoz, J. Muñoz, and M. Rivera, "Fixed-switching-frequency modulated model predictive control for islanded ac microgrid applications," *Mathematics*, vol. 11, no. 3, 2023, Art. no. 672.

[27] J. Xu et al., "Carrier-based modulated model predictive control strategy for three-phase two-level VSIs," *IEEE Trans. Energy Convers.*, vol. 36, no. 3, pp. 1673–1687, Sep. 2021.

[28] C. F. Garcia, C. A. Silva, J. R. Rodriguez, P. Zanchetta, and S. A. Odhano, "Modulated model-predictive control with optimized overmodulation," *IEEE Trans. Emerg. Sel. Topics Power Electron.*, vol. 7, no. 1, pp. 404–413, Mar. 2019.

[29] N. Jin, M. Chen, L. Guo, Y. Li, and Y. Chen, "Double-vector model-free predictive control method for voltage source inverter with visualization analysis," *IEEE Trans. Ind. Electron.*, vol. 69, no. 10, pp. 10066–10078, Oct. 2022.

[30] M. Aly et al., "Weighting factorless sequential model predictive control method with fixed switching frequency for five-level t-type photovoltaic inverters," in *Proc. IEEE 47th Annu. Conf. Ind. Electron. Soc.*, 2021, pp. 1–6.

[31] F. Carnielutti, M. Aly, M. Norambuena, J. Hu, J. Guerrero, and J. Rodriguez, "Fixed switching frequency model predictive control for parallel inverters in microgrids," *Eletrônica de Potência*, vol. 29, Sep. 2024, Art. no. e202430.

[32] Q.-C. Zhong, "Robust droop controller for accurate proportional load sharing among inverters operated in parallel," *IEEE Trans. Ind. Electron.*, vol. 60, no. 4, pp. 1281–1290, Apr. 2013.

[33] T. Nurminen, R. Mourouvin, M. Hinkkanen, and J. Kukkola, "Multifunctional grid-forming converter control based on a disturbance observer," *IEEE Trans. Power Electron.*, vol. 39, no. 10, pp. 13023–13032, Oct. 2024.

[34] F. Sadeque, D. Sharma, and B. Mirafzal, "Seamless grid-following to grid-forming transition of inverters supplying a microgrid," in *Proc. 2023 IEEE Appl. Power Electron. Conf. Expo.*, 2023, pp. 594–599.

[35] M. Gursoy, F. Sadeque, F. Fateh, and B. Mirafzal, "Direct control methods for grid-forming and grid-following inverters," in *Proc. 2023 IEEE Energy Convers. Congr. Expo.*, 2023, pp. 1081–1088.

[36] A. Alassi, K. Ahmed, A. Egea-Alvarez, and C. Foote, "Modified grid-forming converter control for black-start and grid-synchronization applications," in *Proc. 56th Int. Universities Power Eng. Conf.*, 2021, pp. 1–5.

[37] L. S. Araujo and D. I. Brandao, "Self-adaptive control for grid-forming converter with smooth transition between microgrid operating modes," *Int. J. Elect. Power Energy Syst.*, vol. 135, 2022, Art. no. 107479.
[38] S. Geng and I. A. Hiskens, "Unified grid-forming/following inverter control," *IEEE Open Access J. Power Energy*, vol. 9, pp. 489–500, 2022.
[39] R. Teodorescu, M. Liserre, and P. Rodriguez, *Grid Converters for Photovoltaic and Wind Power Systems*. Hoboken, NJ, USA: Wiley, 2007.

Fernanda Carnielutti (Member, IEEE) received the bachelor's, master's, and doctoral degrees in electrical engineering from the Federal University of Santa Maria, UFSM, Brazil, in 2010, 2012, and 2015, respectively.

From 2016 to 2018, she was a Professor with the Federal University of Santa Maria, UFSM - Campus Cachoeira do Sul, Brazil. She is currently a Professor with the Federal University of Santa Maria, UFSM - Campus Santa Maria, Researcher with the Power Electronics and Control Research Group, GEPOC, Researcher with the Institute of Smart Grids, INRI (both at UFSM), and Member of the of the IEEE Power Electronics, Industrial Electronics and Industry Application Societies. Her research interests include modulation of static power converters, multilevel converters power electronics for renewable energies, and model predictive control.

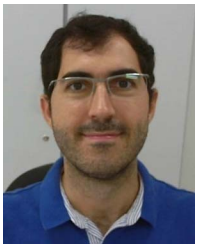

Tiago Davi Curi Busarello (Senior Member, IEEE) received the master's and Ph.D. degrees in electrical engineering from the State University of Campinas, Campinas, Brazil, in 2013 and 2015, respectively.

He has been a Professor with the Federal University of Santa Catarina, Brazil, since 2016. From 2022 to 2023, he was a Postdoctoral Researcher with the University of Vaasa, Finland. In 2014, he was a Visiting Researcher with the Colorado School of Mines, USA. He has authored the book *Power Electronic Converters and Systems*, published by IET in 2024. His research interests include digital control for power electronics and digital twins.

Dr. Busarello is a Member of the IEEE Power Electronics Society.

Ênio Costa Resende received the bachelor's degree in electrical engineering from the Federal University of Uberlândia (UFU), Brazil, including an exchange period with Sacramento State University (SAC State), Sacramento, CA, USA, through the Science Without Borders (CsF/CAPES) program in 2018, and the M.Sc. and Ph.D. degrees in electrical engineering with a specialization in power electronics from the Power Electronics Research Center (NUPEP), UFU, in 2020 and 2024, respectively.

He is currently working on microgrid control and integration. His research interests include islanding detection, distributed generation, renewable energy systems, maximum power point tracking (MPPT), control methods, and power quality.

Qudrat Ullah received the master's degree in electrical engineering from the Northwestern Polytechnical University, Xi'an, China, in 2022.

He is a Project Researcher and doctoral student with the University of Vaasa, Finland, in the field of electrical engineering specializing in advanced control schemes for power electronic converters. With expertise in designing and optimizing control strategies, he focuses on enhancing the efficiency and stability of the modern power systems. His research interests include integrating innovative techniques for renewable energy applications and microgrids.

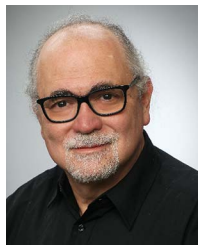

Marcelo Godoy Simões (Fellow, IEEE) received the B.Sc. and the M.Sc. degrees in electrical engineering from the University of São Paulo, Brazil, in 1985 and 1990, respectively, the Ph.D. degree in electrical and computing engineering from The University of Tennessee, USA, in 1995, and the D.Sc. degree (Livre-Docência) in electrical engineering from the University of São Paulo in 1998.

He works as a Professor in flexible and smart power systems with the University of Vaasa, Finland, since 2021. He is a pioneer to apply neural networks and fuzzy logic in power electronics, motor drives, and renewable energy systems. His fuzzy logic-based modeling and control for wind turbine optimization is used as a basis for advanced wind turbine control and it has been cited worldwide. His leadership in modeling fuel cells is internationally and highly influential in providing a basis for further developments in fuel cell automation control in many engineering applications. He made substantial and lasting contribution of artificial intelligence technology in many applications, power electronics and motor drives, fuzzy control of wind generation system, such as fuzzy logic-based waveform estimation for power quality, neural network-based estimation for vector-controlled motor drives and integration of alternative energy systems to the electric grid through AI modeling-based power electronics control. His current research interests include power electronics, power systems, power quality, smart-grid, and renewable energy systems.

Dr. Simões was an US Fulbright Fellow for AY 2014-15, working for Institute of Energy Technology, Aalborg University, Denmark. He was elevated to the grade of IEEE Fellow, with the citation: "for applications of artificial intelligence in control of power electronics systems."